

Cold-Air Pooling in the Upper Douro Valley: An Observational Study

MICHAEL G. SANDERSON,^a MARTA TEIXEIRA,^b AND ANTÓNIO GRAÇA^b

^a *Met Office, Exeter, Devon, United Kingdom*

^b *Sogrape Vinhos, Aldeia Nova, Avintes, Portugal*

(Manuscript received 17 December 2021, in final form 5 October 2022)

ABSTRACT: Cold-air pools can have several different impacts on viticulture, including final grape quality and yields. This study focuses on cold pools in the upper Douro Valley, which is one of the most important viticultural regions of northern Portugal. First, digital elevation model data were analyzed to identify pixels corresponding to the valley floors of the Douro and selected side valleys. Next, the topographic amplification factor was calculated for each of these pixels. Down-valley gradients in the topographic amplification factor were used to identify locations where cold air in the valley was likely to pool. High-time-resolution meteorological data recorded between January 2011 and December 2017 were analyzed to identify cold-pool events at one location in the main Douro Valley. The cold pools were assigned to seven different categories on the basis of their temporal behavior. There was a clear seasonal cycle in numbers of cold pools, with most observed during winter and the fewest in summer. The maximum strengths of the cold pools could occur at any time during the night, although the majority peaked around the middle of the night. This study is believed to be the first to examine cold pools in the upper Douro Valley.

KEYWORDS: Europe; Wind; Cold pools; Surface temperature; Surface observations

1. Introduction

During calm, clear nights, air in contact with the ground becomes cooled via radiative energy loss. As the cooled air is denser than the free atmosphere at the same elevation, it sinks under gravity into valley bottoms and hollows. The air at the valley floor continues to cool via outgoing longwave radiation and becomes cooler than the surrounding air. The resulting stable stratification prevents the air at the valley floor from mixing with the atmosphere aloft while the surrounding valley sides prevents horizontal displacement. Cold-air pooling (CAP) occurs where this cooled air collects on the landscape (Lundquist et al. 2008). Cold pools can be characterized as diurnal, forming during the evening or night and decaying following sunrise the next day, or as persistent, lasting for longer than a day (Whiteman et al. 2001). Cold-air pools can have important impacts on viticulture. Cold-air pooling during winter and early spring could be beneficial to wine growers in the upper Douro Valley of Portugal. The lower temperatures within cold pools would delay budburst, which would compensate for the acceleration of the vine growth cycle resulting from high local temperatures during summer. However, cold pools could also lengthen periods of fog or frost, and delay melting of ice and snow. Frosts are

particularly damaging to vines (Sluys 2006). During the early winter, frosts can damage leaves and reduce the availability of carbohydrates. Frosts following budburst can kill emerging buds and their shoots as well as any developing fruit on the vines.

Temperature and water availability influence grape yields and are responsible for a balanced grape ripening (Fraga et al. 2018). If the summer was particularly hot and dry, cold pools during the ripening season (August–October in the Northern Hemisphere) could be beneficial by reducing heat stress of the vines and improving final grape quality. Cold pools have been recorded during this period in the Walla Walla Valley viticultural area in the northwestern United States (Pogue and Dering 2008).

The rate of change of temperature along a valley is partly controlled by the valley shape, specifically its width, height, and cross-sectional area (McKee and O'Neal 1989; Arduini et al. 2017). Cross sections vary along the length of the valley, resulting in different heating and cooling rates. If the same net radiation flux occurs across the top of a valley as the surrounding plain, the temperature change (and diurnal temperature range) within the valley will be greater than the surrounding plain, because the valley contains a smaller enclosed volume of air (McKee and O'Neal 1989; Whiteman 1990). This effect is quantified by the topographical amplification factor (TAF), which represents the fractional gain in cooling of the air within the valley in comparison with a column of air with the same width (McKee and O'Neal 1989). The TAF is mostly applicable to nighttime conditions; during the daytime, solar warming leads to unstable conditions and vertical mixing.

When the TAF decreases in the down-valley direction (i.e., the valley widens), air cools faster in the higher valley than lower valley owing to the smaller volume of air, which leads to a horizontal pressure gradient that drives nocturnal winds

 Denotes content that is immediately available upon publication as open access.

 Supplemental information related to this paper is available at the Journals Online website: <https://doi.org/10.1175/JAMC-D-21-0263.s1>.

Corresponding author: Michael Sanderson, michael.sanderson@metoffice.gov.uk

DOI: 10.1175/JAMC-D-21-0263.1

© 2022 American Meteorological Society. For information regarding reuse of this content and general copyright information, consult the [AMS Copyright Policy](#) (www.ametsoc.org/PUBSReuseLicenses).

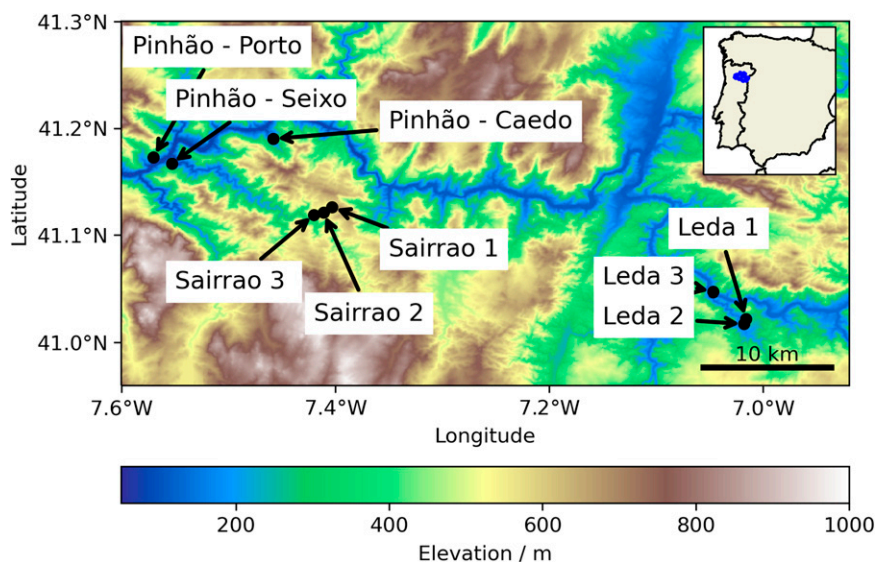


FIG. 1. Terrain height (m) in the upper Douro Valley based on SRTM data with a resolution of 3 arc s (approximately 90 m). The names and locations of nine weather stations operated by Sogrape Vinhos are shown. The inset map shows the border of Portugal and the location of the DDR (blue area), in which the study area is located. The study area size is 57 km \times 38 km.

down the valley (Lundquist et al. 2008; Miró et al. 2010). In this case, the valley is defined as “draining.” If the TAF increases in the down-valley direction (i.e., the valley narrows), the down-valley flow is inhibited, promoting pooling of colder air (McKee and O’Neal 1989; Whiteman 1990); such valleys are defined as “pooling” (Arduini et al. 2017). Lundquist et al. (2008) used gradients in the TAF to map areas of cold-air pooling in three different mountain valley systems.

Here, we present an observational study of cold-air pooling in the upper Douro Valley of northern Portugal. The aims of this study are (i) to identify regions where cold pools could form in the main Douro channel and its tributaries, and (ii) describe the characteristics of any cold pools in those areas.

2. Investigation area, data, and methods

a. Study area

Cold-air pooling is investigated in the upper Douro Valley, within the Douro Demarcated Region (DDR). The DDR is one of the most important wine-making regions in Portugal, responsible for about 20% of all wine produced in Portugal (Instituto da Vinha e do Vinho 2018). The study area (Fig. 1) lies across two subregions of the DDR, Cima Corgo and Douro Superior, and is mostly characterized by narrow valleys and steep slopes. The DDR has a Mediterranean climate, with hot dry summers and mild winters (Cunha et al. 2011). The study region is particularly arid, receiving between 400 and 800 mm of rain per year, mostly in autumn and winter. Frosts are a rare occurrence but are not unheard of. The elevation ranges from approximately 80 m to nearly 1000 m. Vineyards are planted up to 700 m in altitude on terraced slopes and are not irrigated (Cunha and Richter 2020). The

best wines have traditionally been obtained at lower altitudes, where temperatures are highest during the summer (Magalhães 2015).

b. Instrumentation

Sogrape Vinhos, a major producer of wines in Portugal, operate nine weather stations within vineyards in the upper Douro Valley (Fig. 1; Table 1). These stations meet WMO standards for both the instrumentation and siting (e.g., away from obstacles that could shade the station and heat sources such as concrete surfaces). Data from these stations are used to routinely monitor local weather conditions in the vineyards. Forecasts of grape production levels and harvest dates are made by combining these local weather observations with a statistical model derived from grape yield, quality, and grapevine phenology in previous years (e.g., Fontes et al. 2016). Daily totals and means of several climate variables from all nine weather stations form part of the European Climate Assessment

TABLE 1. Weather stations operated by Sogrape Vinhos in the Douro Valley. The data period (final column) indicates the period of data available for this study.

Name of station	Lat ($^{\circ}$ N)	Lon ($^{\circ}$ W)	Alt (m)	Data period
Leda 1	41.022	7.016	213	2011–17
Leda 2	41.017	7.018	318	2011–17
Leda 3	41.047	7.047	163	2011–17
Pinhão–Caedo	41.190	7.458	210	2011–17
Pinhão–Porto	41.173	7.570	193	2014–17
Pinhão–Seixo	41.167	7.553	199	2014–17
Sairrao 1	41.126	7.403	624	2011–17
Sairrao 2	41.121	7.411	548	2011–17
Sairrao 3	41.119	7.420	426	2011–17

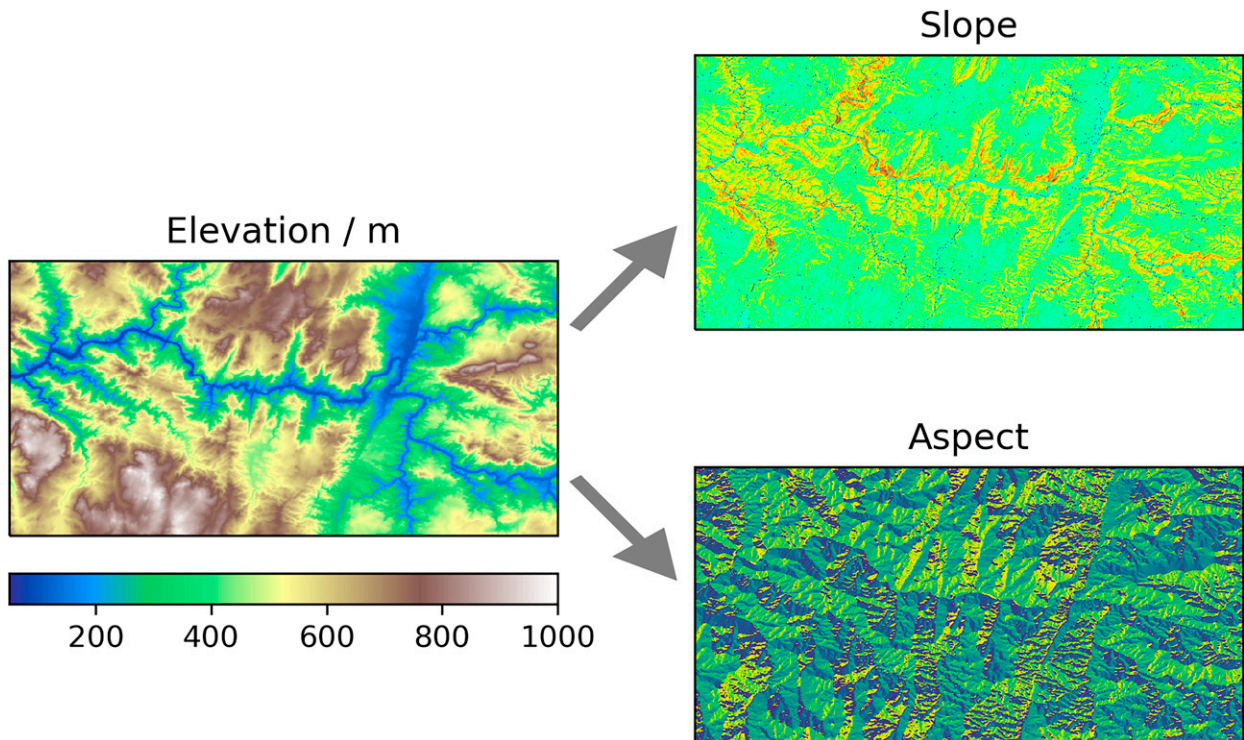


FIG. 2. (left) Elevation data for the upper Douro Valley from the SRTM data, and the (top right) slopes and (bottom right) aspects calculated from the elevation data with pyDEM (Ueckermann et al. 2015). For the slopes, pale blue colors represent the shallowest slopes. Steeper slopes are indicated in yellow and red.

and Dataset (ECA&D; Klok and Klein Tank 2009). The sensors in each weather station are located 2 m above local ground level, and consist of pyranometer (Campbell Scientific CS301), temperature and humidity sensor (Campbell CS215/Hygrovue05) and a leaf-wetting sensor (Campbell 237). In addition, each station includes an anemometer [Environmental Measurements Limited (EML) Wind Speed and Direction 1 (WSD1)] positioned 10 m above the ground and a pluviometer (Pronamic Pro). Data from all sensors are recorded every 15 min. The data series are nearly complete; less than 5% of the observations are missing. The lowest-altitude station (Leda 3) is about 30 m above the level of the Douro River. Consequently, the strength of any temperature inversions around Leda could be underestimated, and some shallow inversions would not be recorded.

The sensors are calibrated four times per year or whenever an anomaly is found. Continuous data quality validation is performed by a third-party academic institution [Instituto de Ciência e Inovação em Engenharia Mecânica e Engenharia Industrial (INEGI), Portugal]. Data quality is first assessed for structural integrity against the database template and then validated against physical limits of each recorded variable. A second step of validation is performed to check for temporal coherence (gap detection), internal coherence (variable correlation), and spatial coherence (comparison with nearby stations). A “present weather code” or similar was not recorded, meaning it is not possible to precisely identify days when frost or fog occurred in the valleys.

c. Topographic data

Terrain heights for the study area were extracted from the Digital Elevation–Shuttle Radar Topography Mission (SRTM), version 4.1, which has a horizontal resolution of 3 arc s, or 90 m (Jarvis et al. 2008). Any missing data have been infilled following the method of Reuter et al. (2007). The data are in the form of a raster array, where the value of an element in the array gives the elevation of that point. The terrain heights are available to the nearest whole meter.

d. Identification of river channels in the SRTM data

To calculate the topographical amplification factor along the Douro Valley and tributaries, the pixels in the SRTM data corresponding to the floors of the valley and its tributaries need to be identified in the down-valley direction. These pixels were found using the pyDEM package (Ueckermann et al. 2015; see the appendix). First, the magnitudes of the slopes of the SRTM data and their directions (or aspects) were calculated (Fig. 2). The slopes and aspects are used within pyDEM to calculate flow directions between pixels and the upstream contributing area using the D^∞ method of Tarboton (1997). A connectivity (or adjacency) matrix is constructed as part of this calculation. The value in row i and column j of this matrix represents the fraction of the area of pixel j that drains into pixel i (Ueckermann et al. 2015). Hence, by starting at a pixel located at the head of a tributary and following the main drainage route in the connectivity

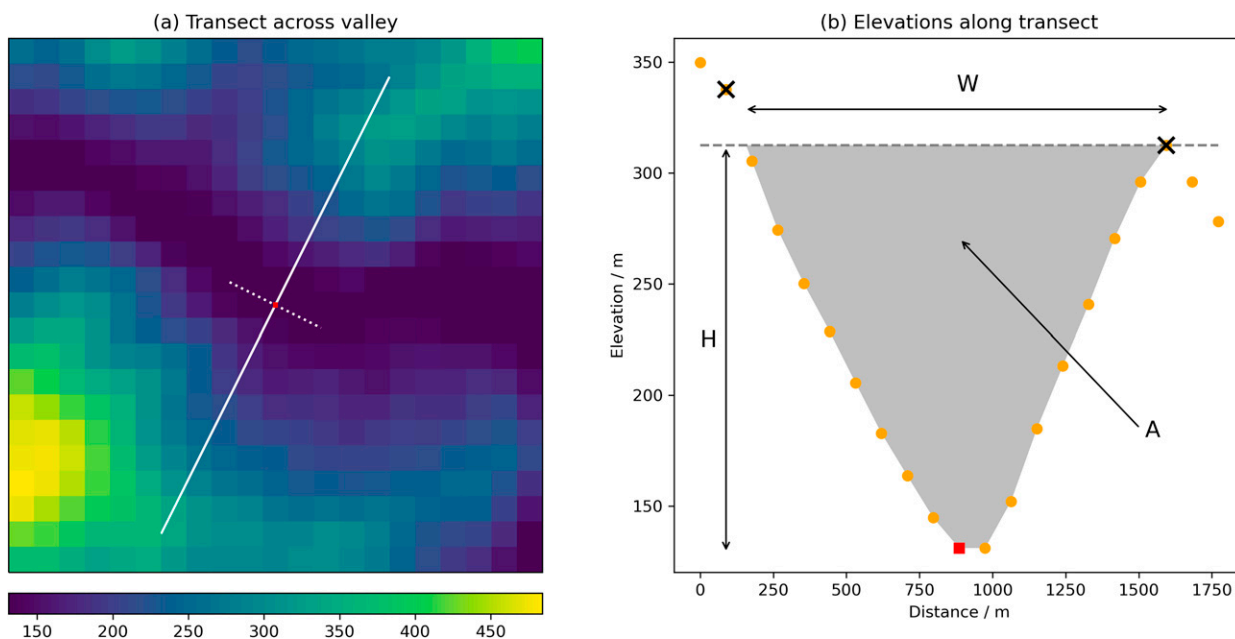


FIG. 3. (a) Example of a transect across the main valley of the Douro. The river valley floor is indicated by the dark purple colors; pale blue and yellow colors indicate higher elevations (as shown by the color bar). A straight line fitted to five contiguous pixels along the valley floor is shown by the dotted white line. The center pixel is indicated by the red square. The transect across the valley, which is perpendicular to the dotted line and fitted through the center pixel, is shown by the solid white line. (b) Calculation of valley width W , height H , and cross-sectional area A from the transect. Elevations along the transect are shown by the solid orange circles, and the lowest point on the cross section is indicated by the red square. The elevation of the valley top is shown by the dashed gray line. The two crosses indicate the points on the transect that contain the valley. The gray-shaded area illustrates the valley cross-sectional area A , which was computed using the trapezium rule.

matrix, the pixels corresponding to the valley floor can be identified in the down-valley direction.

Pixels along the main valley of the Douro were identified manually. A series of dams were built along much of the Douro in the 1970s (Mayson 2019). The elevations of the valley floor in the DEM data are the same along large sections. Consequently, pyDEM cannot be used because there is no change in elevation between adjacent pixels.

In the SRTM data, the elevations of the floors of the Douro and its tributaries do not descend continuously. In some places, the elevations of the floors of the tributaries increase slightly before falling once more. These areas are treated as flat regions (or “flats”) within pyDEM. The total area contributions that drain into a flat region are collected, and then distributed proportionally to pixels at the edge of the flat, depending on the difference in elevation between the flat region and surrounding pixels (Ueckermann et al. 2015). The coordinates of pixels within the flat region are not included in the connectivity matrix.

The A* search algorithm (Hart et al. 1968; Dechter and Pearl 1985; see the appendix) was used to identify the pixels corresponding to the valley floor within each flat region. Briefly, the A* algorithm aims to find a path between two nodes (here, pixels in the SRTM data) that has the lowest cost. In the present study, each of the eight pixels surrounding a node (i.e., the central pixel) in the SRTM data are considered equally likely to be part of the optimal path. The cost of

moving from a node to a surrounding pixel is set equal to the elevation of the surrounding pixel. In this way, the A* algorithm was able to identify a path following the valley floor through the flat regions. The pixels along these paths were then combined with those found with pyDEM to produce a continuous sequence of pixels in the down-valley direction. Pixels along the tributaries identified using pyDEM and the A* algorithm are shown in Fig. S1 in the online supplemental material.

e. Calculation of the TAF

The TAF may now be calculated at all points along the valley floors using the pixels identified in the previous step. A straight line was fitted through the coordinates of groups of five adjacent pixels, to represent the local direction of the valley (Fig. 3a, dotted white line). The gradient of a line perpendicular to the first was calculated and fitted through the central pixel. A transect across the valley was created by extending the perpendicular line either side of the central pixel. A radius of 10 pixels (approximately 900 m) was used for the two tributaries of the Douro, as shown by the solid white line in Fig. 3a. A larger radius of 20 pixels was used for the main channel of the Douro. Elevations along the transect (Fig. 3b, solid orange circles) were found via bilinear interpolation of the SRTM data. If part of the transect was orientated along the main river channel (owing to meanders) or a tributary,

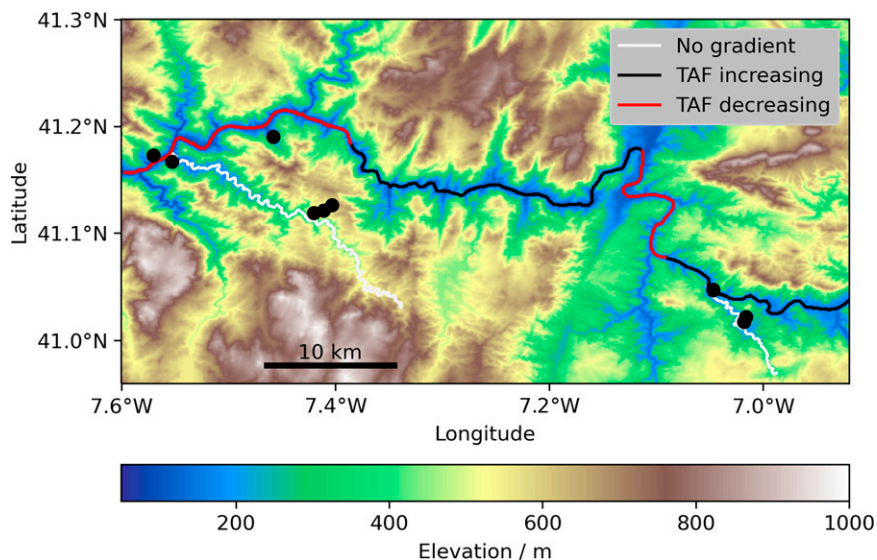


FIG. 4. Gradients in the TAF in the down-valley direction. Increasing and decreasing gradients are shown by black and red lines, respectively. All gradients were significant at the 5% level. The gradients in the TAF along two of the tributaries linking the weather stations at Sairrao and Pinhão and Leda (shown by the pale gray lines) are indistinguishable from zero. The solid circles indicate the positions of the weather stations (Fig. 1; Table 1).

the transect was rotated about the central point by a small angle and the elevations recalculated.

A local maximum was searched for in the elevations on one or both sides of the valley. The valley top was defined as the lower of the two maxima (Lundquist et al. 2008), as shown by the \times symbols in Fig. 3b. The valley height H was calculated as the vertical distance between the valley top and the lowest elevation of the transect (Fig. 3b). The valley width W was calculated from the coordinates of the two edges using the Haversine formula (Smart 1990). The cross-sectional area of the valley A was calculated from the transect using the trapezium rule. The TAF was calculated at all points along the valleys using the formula: $TAF = WH/A$ (Whiteman 1990; Lundquist et al. 2008; Arduini et al. 2017). The gradients of the TAF in the down-valley direction were found using simple least squares, and statistical significance of the gradients was computed at the 5% level.

f. Identification of cold-air pooling events

At least two weather stations are needed to record cold pools, one on or close to the valley floor and a second at a higher altitude. In this study, there are two locations where weather stations are located near the valley floor of the Douro and higher within the valley: Sairrao 3–Pinhão Seixo, and Leda 3–Leda 2 (Fig. 1; Table 1). In addition, data from the station Sairrao 1, located on top of a hill above the main channel of the Douro, represents conditions above the valleys.

For each date in the weather station records, temperatures from 1200 LT on the previous day to 1200 LT on the chosen date were extracted, which encompasses all data recorded during the night and early morning after sunrise. Days with

less than 90% of valid (i.e., nonmissing) data, either during the whole 24-h period or just the night, were not analyzed. Here, the night is defined as the period between sunset and sunrise. The vertical temperature gradient was calculated for all times. An initial set of cold pools was identified as nights and early mornings with a temperature inversion of at least 1°C (Jemmett-Smith et al. 2018).

3. Results

a. Gradients in the TAF

The majority of the TAF values along the main channel of the Douro were between 1.4 and 2.0 (Fig. S2 in the online supplemental material), which are expected for U- and V-shaped valleys (Whiteman 1990). In a few parts of the valley, the TAF was larger, between 2.0 and 2.8, reflecting the slightly convex shape of the valley sides. Gradients in the TAF along the Douro and the tributary between the stations at Sairrao and Pinhão in the down-valley direction are shown in Fig. 4 and supplemental Fig. S2. The general gradient in TAF along different parts of the valley was determined by eye, following Lundquist et al. (2008). All gradients, both positive and negative, were significant at the 5% level. The Douro Valley narrows as it reaches the stations at Leda, resulting in a positive gradient in the TAF. The gradient in the TAF is positive farther along the Douro Valley, where it again narrows (Fig. 4, solid black lines). The gradients in the TAF are negative in other parts of the valley (Fig. 4, solid red lines). The gradients in the TAF along the tributaries linking the stations of Sairrao 3 and Pinhão–Seixo, and Leda (pale gray lines) are very small and negative and are not significant.

Cold-air pooling is therefore possible at Leda and a second location in the Douro Valley below the station Sairrao 1 (Fig. 1). Because there are no stations at the latter location, the analysis will focus on data recorded at Leda.

b. Cold-pool characteristics

Cold pools were initially identified on 901 nights (34% of all nights) at Leda. The temporal profiles of the temperatures from both stations (Leda 2 and Leda 3) on those nights were examined, leading to 67 being rejected for several reasons: When cold pools occur, temperatures at both stations, especially the one close to the valley floor, should fall during part of or all of the night (e.g., Fig. 2 in [Dorninger et al. 2011](#)). In the present study, there were a small number of occasions when temperatures at both stations increased throughout the night, indicating no cold pooling occurred. On other occasions, an apparent cold pool was caused by a short-lived warming event that occurred during the night at the upper station (Leda 2). Temperatures at both stations either side of the warming event were very similar, again indicating a cold pool had not formed. Similarly, a few possible cold pools were the result of a rapid increase in temperature at the higher-altitude station immediately after sunrise. During the preceding nights, the temperatures at both stations were similar. The rate of erosion of cold pools is determined by wind speeds above the cold pool and the temperature inversion strength within the cold pool ([Zhong et al. 2003](#)). Erosion of the cold pool would result in the upper station (Leda 2) emerging above the pool (and a corresponding increase in temperature) while the lower station (Leda 3) would remain within the cold pool for a few hours. Other possible factors for the delay in temperature increase at the lower station are shading of the valley floor and the presence of mist or fog.

On other nights, an apparent cold pool lasted less than a few hours, and had ended before the lowest temperatures were recorded. Most of the temperature differences between the two stations were only a few tenths of a degree. Temperature gradients between Leda 2 and Sairrao 1 were calculated in addition to the gradients between Leda 3 and Leda 2. On some nights, the cold pool (i.e., positive gradient between Leda 3 and Leda 2) was confined to the lower valley. The temperature gradient between Leda 2 and Sairrao 1 remained negative throughout those nights, and was mostly smaller than 1°C. On other nights, a weakly positive temperature gradient was present for a few hours between Leda 3 and Leda 2 as well as between Leda 2 and Sairrao 1, suggesting a deeper cold pool occurred for a short period of time. Except for these events, the gradient between Leda 2 and Sairrao 1 was negative. These events were too brief and the temperature gradients too weak to be clear evidence of cold-air pooling, and so were not included. On a small number of nights, there was considerable variability in temperatures at one or both of Leda 2 and Leda 3, and the temperatures overlapped. It was difficult to say whether a cold pool had occurred on these nights, and so they were also rejected. These checks led to a final set of 834 cold pools (32% of nights).

All of the cold pools identified at Leda were diurnal. None lasted for more than a day, although a few lasted well into the daytime. For example, on 30 January 2013, a cold pool formed at the start of the night, and temperatures at Leda 3 (lower station) were lower by 1°C or more than Leda 2 throughout the night, remaining so until local noon on 31 January. Around an hour before sunset on 31 January, temperatures at Leda 3 fell below those at Leda 2 and remained lower until a few hours after sunrise.

1) COLD-POOL STRENGTHS AND FREQUENCIES

The cold-pool strength is defined as the maximum temperature difference between the two stations over the course of the cold-pool event, and so corresponds to the maximum vertical temperature gradient. The distribution of cold-pool strengths at Leda is shown in Fig. 5a. Strong cold pools, defined as those with strengths greater than 4°C ([Jemmett-Smith et al. 2018](#)), only represented 4% of all events. The greatest cold-pool strength recorded was 5.5°C. The number of cold pools in each year is shown in Fig. 5b. Air masses in spring 2011 in the upper Douro Valley were anomalously warm, meaning any cold pools would be weak and shallow. Very few cold pools in this year had gradients larger than 4°C. Strong cold pools occurred in all years, and the largest numbers were seen in 2015 and 2017. Cold pools occur throughout the year, as shown in Fig. 5c, and there is a clear seasonal cycle in their numbers. The majority of cold pools occur in winter and early spring (January–March), and the smallest numbers are seen in the warmer months (May–September). Similar seasonal cycles in cold-pool numbers were observed in northern Finland by [Pepin et al. \(2009\)](#), and at two locations in Oregon in the northwestern United States: the Columbia River basin ([McCaffrey et al. 2019](#)) and a forested valley ([Rupp et al. 2020](#)).

Strong pools (greater than 4°C) are seen in most months, but the largest numbers occur between December and March. The strongest cold pools were not necessarily present on the coldest days. For example, on 18–19 January 2017, easterly winds advected very cold air from Europe and Russia to northern Portugal. Nighttime temperatures at the stations Leda 3 and Leda 2 were close to or below freezing, and the cold-pool strengths were between 2° and 3°C.

The time at which the maximum cold-pool strength occurred relative to local sunrise is shown in Fig. 5d. Cold-pool strengths can peak at any time during the night, although the majority reach their maximum strength between 5 and 9 h before sunrise. A secondary maximum in the numbers of cold pools can be seen in the few hours following sunrise, probably due to erosion of the cold pool where the upper station emerges into the boundary layer, but the lower station remains within the cold pool for a longer period. Heating of the valley floor by sunlight and dissolution of the cold pools would be further delayed by the presence of frost or fog. Cold winter fogs have become more common in the Douro Valley following the building of a number of dams along its length during the 1970s ([Mayson 2019](#)). In the study area, the valley floor is the River Douro, which would modify the vertical

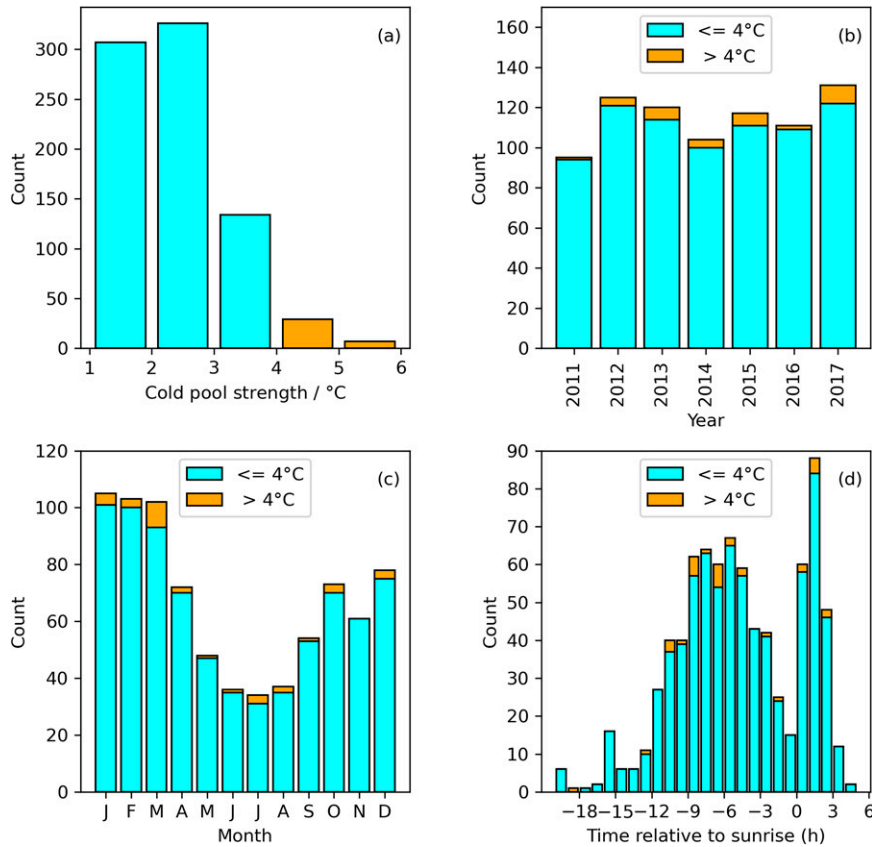


FIG. 5. Characteristics of cold-air pools at Leda: (a) number of cold pools as a function of their maximum strength, (b) number of cold pools and strong pools in each year, (c) numbers of cold and strong pools in each month, and (d) numbers of pools and strong pools in each hour relative to local sunrise, using the times at which the maximum strengths were recorded.

temperature structure (Kossmann et al. 2002), although the exact effects of a body of water on cold pools are unclear. The strongest cold pools (with strengths > 4°C; orange bars in Fig. 5d) occur throughout the night, although a larger proportion are seen earlier in the night, 7–9 h before sunrise. Other strong pools continue to develop during the night and reach their maximum strengths after sunrise.

2) COLD-POOL EVOLUTION CATEGORIES

Dorninger et al. (2011) used high-time-resolution temperature measurements from multiple sensors positioned along elevation transects to study cold pools in a basin in the eastern Alps. The cold pools were assigned to one of eight different categories depending on the evolution of temperatures during the night. In the present study, the temporal profiles of temperatures at both stations (Leda 3 and Leda 2) on nights with cold pools were compared with sample profiles presented in Fig. 2 and Fig. 7 of Dorninger et al. (2011) and assigned to one of the eight categories (Table 2). This comparison was not straightforward, because the cold pools strengths in the upper Douro Valley (most are in the range 1°–3°C) were much weaker than those measured by Dorninger et al. (2011) in the Alpine basin (strengths were about 25°C). The temporal

evolution of cold pools observed in the Douro Valley was generally more gradual than the cold pools measured by Dorninger et al. (2011). On many (but not all) nights, the temperatures at both stations reached their lowest values at or shortly before sunrise. A number of the cold pools observed at Leda were weak, and sometimes appeared more than once throughout the

TABLE 2. Numbers of cold pools in each evolution category. The evolution categories a–h were derived by Dorninger et al. (2011), and the marginal category m is described by Mahrt and Heald (2015). Cold pools in the present study were assigned to these categories via a visual comparison, and so the numbers in each category are subjective.

Category	Category name	No. of events
a	Undisturbed evolution	182
b	Late buildup	240
c	Early breakup	79
d	Mixing event	0
e	Upper disturbance	6
f	Lower disturbance	11
g	Layered erosion	0
h	Cold-air-pool window	53
m	Marginal	225

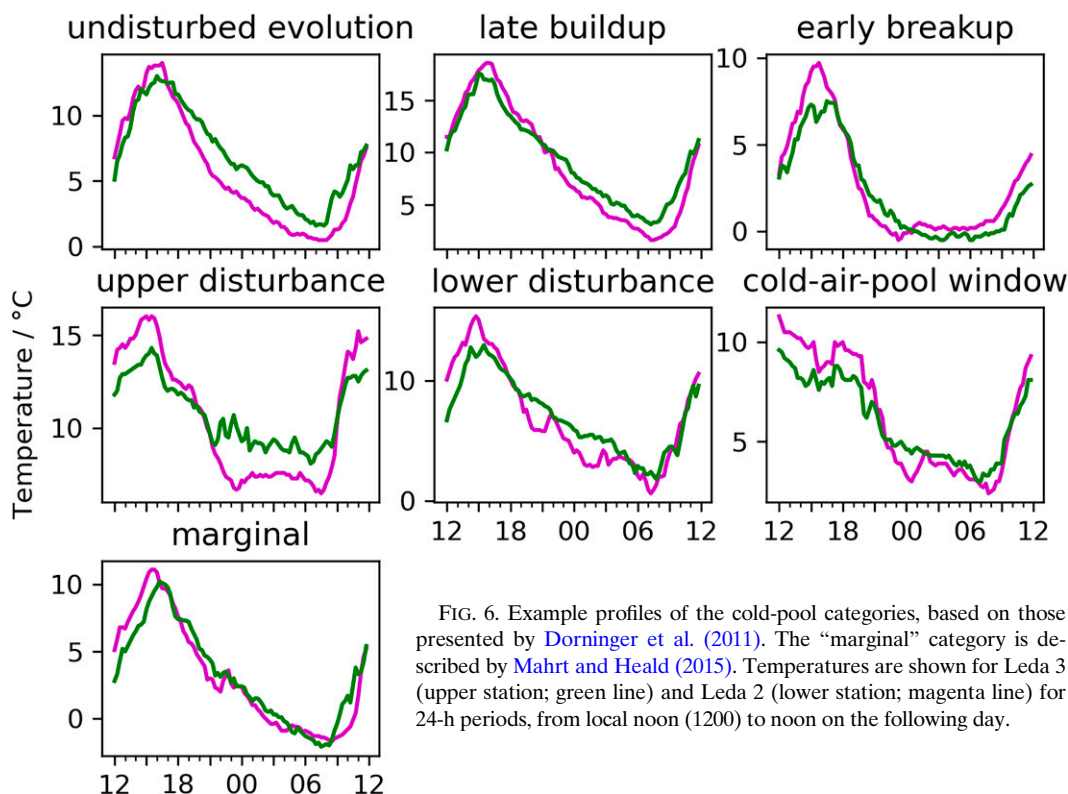


FIG. 6. Example profiles of the cold-pool categories, based on those presented by Dorninger et al. (2011). The “marginal” category is described by Mahrt and Heald (2015). Temperatures are shown for Leda 3 (upper station; green line) and Leda 2 (lower station; magenta line) for 24-h periods, from local noon (1200) to noon on the following day.

night. These latter types were categorized as “marginal,” following the description of such pools by Mahrt and Heald (2015). Example profiles at Leda for each category are shown in Fig. 6, and time series of temperature gradients between the two stations are shown in Fig. S3 in the online supplemental material. The numbers of cold pools in each category are listed in Table 2.

The majority of the cold pools were assigned to the three categories “undisturbed evolution,” “late buildup” and “marginal” (Table 2). In our study, cold pools that started forming before sunrise or within an hour after sunset and that existed throughout the night were classed as “undisturbed evolution.” The category “late buildup” includes all cold pools that began later than an hour after sunset and were still present at sunrise. The example profile for the category “cold-pool window” shown by Dorninger et al. (2011) exhibits a brief downward spike in temperatures that lasted for 1–2 h. A small number of cold pools were assigned to this category when a short-lived drop in temperatures at the lower station (Leda 3) was apparent. In the present study, the cold-pool window was slightly longer, up to 3 h. On a few nights (e.g., 17 February 2011), two cold-pool windows were recorded.

On a small number of nights, considerable variability in temperatures was recorded at the higher station (Leda 2), where temperatures fluctuated by 2°–4°C over a few hours (Fig. 6). The temperature profiles at Leda 3 (valley floor) were smoother and did not exhibit this variability. These nights were tentatively classed as “upper disturbance.” Similarly, nights with high variability in temperatures at the lower station but little or no variability at the upper station were categorized as “lower

disturbance.” In the profiles shown by Dorninger et al. (2011), fluctuations in temperature at the higher stations during cold pools in the “upper disturbance” category were notably larger than fluctuations in temperature at the lower stations during nights classed as “lower disturbance.” In the present study, the fluctuations in temperature in these two categories were of similar magnitude. In the category “layered erosion,” temperature fluctuations were measured within the cold pool (Fig. 2g of Dorninger et al. 2011). It was not possible to identify similar events in the present study because data from only two stations were available. None of the profiles resembled the category “mixing event,” where temperatures increased briefly, especially at the lower station, so that the temperatures at all stations along the transect were very similar (Dorninger et al. 2011).

Nights classed as “upper disturbance” occurred in unstable air masses. For example, on 7–8 January 2011, a deep area of low pressure was located to the northwest of Portugal, which advected cold air from the Arctic over the Atlantic to northern Portugal. Occluded fronts and troughs were advected over northern Portugal in a brisk westerly flow (Fig. S4 in the online supplemental material). The largest fluctuations in temperature measured at Leda coincided with the passage of the fronts and troughs.

3) WIND SPEEDS AND DIRECTIONS

Wind roses showing average nighttime wind speeds and directions for weather stations at Leda 3, Leda 2 and Sairrao 1 are shown in Fig. 7. Sairrao 1 is located on a hilltop above the

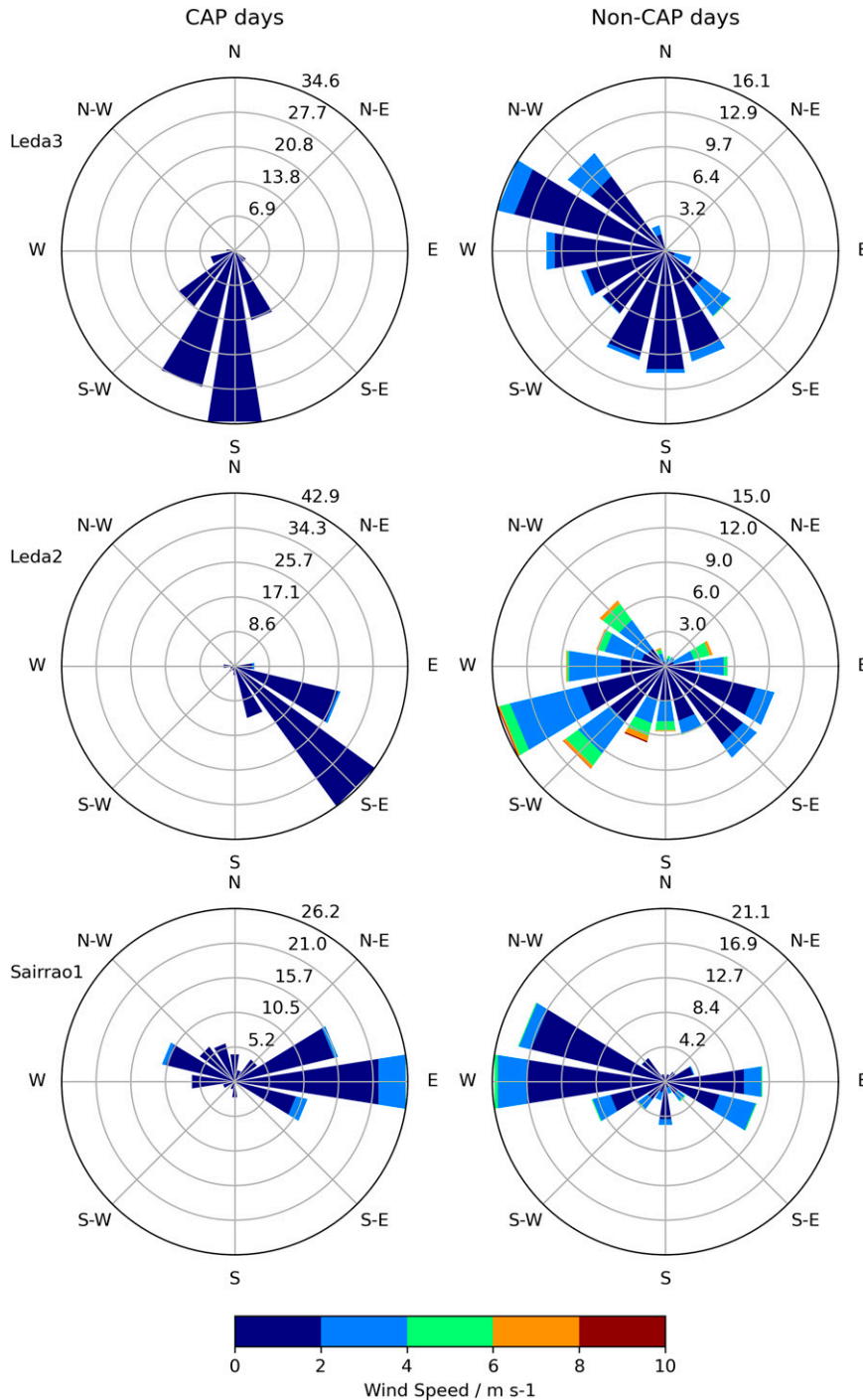


FIG. 7. Percentages of nights as a function of nighttime-averaged wind speed and wind direction recorded at the stations Leda 3, Leda 2, and Sairrao 1, for nights with (left) undisturbed cold pools (CAP days; category “a” in Table 2) and (right) without cold pools (Non-CAP days). Leda 3 and Leda 2 are located near the valley floor and at the top of the valley, respectively (Fig. 1). Sairrao 1 is located on a hilltop above the Douro Valley and represents wind speeds and directions outside the valley.

Douro Valley (Fig. 1; Table 1), and represents conditions outside the valley. The data are shown separately for nights with undisturbed cold pools (category “a” in Table 2) and nights without cold pools. Wind speeds on nights with cold pools (Fig. 7, left column) are low ($<4 \text{ m s}^{-1}$) and are slower than speeds on days without cold pools (Fig. 7, right column), especially at Leda 2.

Wind directions at Leda 3, located near the valley floor, are predominantly from the south southwest and south during nights with cold pools, suggesting airflow down the valley. On nights without cold pools, the wind direction is mainly west northwesterly or northwesterly, indicating flow in the up valley direction. The wind directions at Leda 2 are consistent with this interpretation. On nights with cold pools, the winds are mainly from the southeast, again indicating down-valley flow. On nights without cold pools, the flow is mainly across the valley, having a southwesterly direction.

The wind directions at Sairrao1 are more bimodal in nature, with the majority easterly and westerly (Fig. 7, lower row). On days with cold pools, easterly winds are the predominant type, with smaller proportions from the west. On days without cold pools, the majority of the winds have a westerly or west northwesterly direction. This result may be partly due to correlations between wind direction and temperature. Easterly winds during the colder months are associated with lower temperatures, when cold air would be advected from eastern Europe and Russia to northern Portugal (as happened on 16–17 January 2017, for example). Some westerly winds are also associated with advection of colder air from northern Europe (e.g., 7–8 January 2011; Fig. S4 in the online supplemental material). On other occasions, westerly winds would advect milder air from the Atlantic to northern Portugal. The mountains of northern Portugal are oriented north–south, so most winds would be channeled through the Douro Valley, which is oriented roughly east–west in the central part of the study area (Fig. 1). It is also possible easterly winds could encourage cold-pool formation by increasing the flow of cold air down the valley toward the narrower region just below Leda (Fig. 3). In contrast, westerly winds would counteract any down-valley flow.

4. Discussion and conclusions

Cold-air pooling has been studied in the upper Douro Valley over a period of seven years. Areas where cold-air pooling could occur in the upper Douro Valley were identified by first calculating the topographical amplification factor (TAF) along the Douro Valley and then looking for regions where the gradient in the TAF increased in the down-valley direction. The TAF was calculated from transects across the valley using digital elevation data. The valley sides of the upper Douro are not uniform; in many places there are small side valleys, and the main channel is joined by several tributaries in the study area. The transects were perpendicular to the local valley direction, meaning the estimated valley width (and hence the TAF) increases and decreases between adjacent pixels of the valley floor. Transects with slightly different directions would be equally valid, but would result in different TAF values, depending on whether the

transect coincided with a side valley or a ridge between side valleys. The TAF values for the Douro appear “noisy” (Fig. S2 in the online supplemental material); similar variations in the TAF were shown by Lundquist et al. (2008) along two valleys in the Rocky Mountains.

High-time-resolution temperature measurements recorded by a pair of weather stations in the upper Douro Valley are available for seven years, allowing variation in numbers and strengths of cold pools between years to be studied. The numbers of cold pools and their strengths are qualitative. They will depend on the difference in altitude between the two stations and the horizontal offset with respect to surface features and the shape of the valley sides. The total numbers of cold pools and numbers in each category could be different if one or both of the weather stations were in different locations. In the present study, a cold pool was defined as a night on which the temperature gradient between the two stations (Leda 3 and Leda 2; Table 1) was at least 1°C . Any weaker cold pools would not be included. Some studies used alternative metrics to identify cold pools, including a positive gradient in temperature, virtual temperature or virtual potential temperature with height (Whiteman et al. 2001; Pages et al. 2017; McCaffrey et al. 2019; Rupp et al. 2020). Other studies identified cold pools using a smaller minimum temperature difference between two stations, for example, 0.5°C (Pepin et al. 2009).

The majority of the cold pools in the present study had strengths between 1.0° and 3.0°C , as recorded by two stations (Leda 3 and Leda 2) with an altitude difference of 155 m. A small number of cold pools had strengths up to 5.5°C . Jemmett-Smith et al. (2018) recorded cold pools with greater strengths (up to 9.6°C , although most were 6°C or smaller) during a 10-month period in a valley in Shropshire, United Kingdom. The two stations used had a very similar difference in altitude (160 m) to the present study. In contrast, Dorninger et al. (2011) recorded much stronger cold pools with strengths between 11° and 26°C in a high-altitude ($\sim 1300 \text{ m}$) basin in the Alps. The altitude difference between the highest and lowest dataloggers was 137 m. Pepin et al. (2009) recorded inversions with strengths below 6°C between May and September, but up to 15°C during winter (December–March) in a valley in northern Finland using data from two loggers that were 110 m apart in altitude. Overall, the cold pools recorded at Leda in the upper Douro Valley are weaker than those measured elsewhere.

All of the cold pools identified at Leda were diurnal in nature; none lasted for more than one night, although a few persisted until local noon. There was a clear seasonal cycle in the numbers of cold pools, with the largest numbers recorded in winter and early spring (December–March), and the smallest numbers during summer (June–August). Cold pools reached their maximum strengths throughout the night, with the majority around local midnight.

The cold pools were classified into seven different categories, by comparison of their nocturnal evolution with example profiles from other studies. This classification was mostly done by eye, and the number of pools in each category is therefore subjective. Nevertheless, most cold pools were found to begin just before sunset or during the night and

persisted until sunrise. Marginal cold pools, which were weak and appeared intermittently, occurred 28% of the time. Only very small numbers of the pools exhibited signs of disturbance in their upper or lower layers. On some nights, considerable variability in temperatures was recorded at one or both stations. The causes of these fluctuations, especially those at the lower station, are unclear, although some coincided with the passage of fronts and troughs over the upper Douro area.

An analysis of wind speeds and directions recorded at a station located on a hilltop above the Douro Valley showed that cold pools were more prevalent when wind speeds were low. However, winds with an easterly or northeasterly component were notably more common during nights with cold pools. Easterly winds during winter would be associated with advection of colder air from eastern Europe and Russia. On nights without cold pools, the majority of the winds had a more westerly origin, suggesting advection of milder air from the Atlantic Ocean.

Pepin et al. (2009) found only weak relationships between synoptic indices representing gradient wind strength and flow direction with cold-pool strengths in the Kevo Valley in northern Finland. In this location, the very low sun during winter lead to stabilization of the valley atmosphere and decoupling from the synoptic background. In contrast, a strong influence of the synoptic conditions on cold pools was found in other locations (Miró et al. 2018). The analysis above suggests that cold-pool formation in the Douro Valley is partly controlled by the synoptic conditions.

The weather stations used in the present study are sited within vineyards for monitoring and management purposes. The lower station (Leda 3) is located about 30 m above the level of the Douro River. Cold pools whose depths are smaller than 30 m would not be recorded. The exact effects of the Douro River (a body of water) on the local climate and subsequent formation of cold pools are not known. A number of dams were built along the Douro in the 1970s, turning much of the river into a series of lakes (Mayson 2019), which in turn would modify the temperature of the surface of the water relative to a free-flowing river. One change in the local climate resulting from the building of the dams is an increase in the number of cold winter fogs in the Douro, which become trapped in the valleys (Mayson 2019). No studies are known that have addressed the effects of a large and relatively placid body of water on cold pools during winter.

Acknowledgments. This work was supported by the project MED-GOLD, which received funding from the European Union's H2020 Research and Innovation Programme under Grant Agreement 776467.

Data availability statement. The SRTM 90-m digital elevation (DEM) data were obtained online (<https://srtm.csi.cgiar.org/>). The data are provided in mosaicked $5^\circ \times 5^\circ$ tiles. All tiles were downloaded and combined into a single file. DEM data for the study region were then extracted from the single file. Because of the commercially sensitive nature, the supporting weather station data cannot be made openly available. Further information about the data and conditions for access

are available via the European Climate Assessment and Dataset (<https://www.ecad.eu/dailydata/index.php>).

APPENDIX

Software

Two software packages, pyDEM and the A* algorithm, were used in this study. They were obtained from two different sources as shown below.

The pyDEM package was downloaded from github (<https://github.com/creare-com/pydem>). pyDEM is written in Python 2; a small number of changes were made by one author (Sanderson) for execution with Python 3.6. The paper describing pyDEM is available online (http://conference.scipy.org/proceedings/scipy2015/mattheus_ueckermann.html).

An implementation of the A* algorithm in Python written by V. Batočanin was obtained online (<https://stackabuse.com/basic-ai-concepts-a-search-algorithm/>). It was modified by one author (Sanderson) to work with gridded data.

REFERENCES

- Arduini, G., C. Chemel, and C. Staquet, 2017: Energetics of deep Alpine valleys in pooling and draining configurations. *J. Atmos. Sci.*, **74**, 2105–2124, <https://doi.org/10.1175/JAS-D-16-0139.1>.
- Cunha, M., and C. Richter, 2020: Climate-induced cyclical properties of regional wine production using a time-frequency approach in Douro and Minho wine regions. *Ciência e Técnica Vitivinícola*, **35**, 16–29, <https://doi.org/10.1051/ctv/20203501016>.
- Cunha, S., and Coauthors, 2011: *Atlas Climático Ibérico*. Instituto de Meteorologia de Portugal, 80 pp., https://www.ipma.pt/resources.www/docs/publicacoes.site/atlas_clima_iberico.pdf.
- Dechter, R., and J. Pearl, 1985: Generalized best-first search strategies and the optimality of A*. *J. Assoc. Comput. Mach.*, **32**, 505–536, <https://doi.org/10.1145/3828.3830>.
- Dorminger, M., C. D. Whiteman, B. Bica, S. Eisenbach, B. Pospichal, and R. Steinacker, 2011: Meteorological events affecting cold-air pools in a small basin. *J. Appl. Meteor. Climatol.*, **50**, 2223–2234, <https://doi.org/10.1175/2011JAMC2681.1>.
- Fontes, N., J. Martins, and A. Graça, 2016: Study of agrometeorological measurements on “terroirs” of Alentejo wine region: Impact on grape yield and harvest date variation. *10th Symp. of the Vitiviniculture of Alentejo*, Évora, Portugal, ATEVA, 137–146, https://www.ateva.pt/ateva_site_media/cms_page_media/75/LIVRO%20DE%20ACTAS%20VOL.2.pdf.
- Fraga, H., R. Costa, and J. Santos, 2018: Modelling the terroir of the Douro demarcated region, Portugal. *E3S Web Conf.*, **50**, 02009, <https://doi.org/10.1051/e3sconf/20185002009>.
- Hart, P. E., N. J. Nilsson, and B. Raphael, 1968: A formal basis for the heuristic determination of minimum cost paths. *IEEE Trans. Syst. Sci. Cybern.*, **4**, 100–107, <https://doi.org/10.1109/TSSC.1968.300136>.
- Instituto da Vinha e do Vinho, 2018: Vinhos e Aguardentes de Portugal, Anuário 2018 (Wines and Spirits of Portugal, Yearbook 2018). Ministério da Agricultura, do Desenvolvimento Rural e das Pescas, 206 pp., [https://www.ivv.gov.pt/np4/%7B\\$clientServletPath%7D/?newsId=1736&fileName=IVV_BAIXAQ_vf.pdf](https://www.ivv.gov.pt/np4/%7B$clientServletPath%7D/?newsId=1736&fileName=IVV_BAIXAQ_vf.pdf).
- Jarvis, A., H. I. Reuter, A. Nelson, and E. Guevara, 2008: Hole-filled seamless SRTM data V4. International Centre for

- Tropical Agriculture, CGIAR, accessed 26 November 2008, <https://srtrm.cgiar.org>.
- Jemmett-Smith, B., A. N. Ross, and P. Sheridan, 2018: A short climatological study of cold air pools and drainage flows in small valleys. *Weather*, **73**, 256–262, <https://doi.org/10.1002/wea.3281>.
- Klok, E. J., and A. M. G. Klein Tank, 2009: Updated and extended European dataset of daily climate observations. *Int. J. Climatol.*, **29**, 1182–1191, <https://doi.org/10.1002/joc.1779>.
- Kossmann, M., A. P. Sturman, P. Zawar-Reza, H. A. McGowan, A. J. Oliphant, I. F. Owens, and R. A. Spronken-Smith, 2002: Analysis of the wind field and heat budget in an alpine lake basin during summertime fair weather conditions. *Meteor. Atmos. Phys.*, **81**, 27–52, <https://doi.org/10.1007/s007030200029>.
- Lundquist, J. D., N. Pepin, and C. Rochford, 2008: Automated algorithm for mapping regions of cold-air pooling in complex terrain. *J. Geophys. Res.*, **113**, D22107, <https://doi.org/10.1029/2008JD009879>.
- Magalhães, N., 2015: *Tratado de Viticultura: A Videira, a Vinha e o "Terroir."* 2nd ed. Esfera Poética, 607 pp.
- Mahrt, L., and R. Heald, 2015: Common marginal cold pools. *J. Appl. Meteor. Climatol.*, **54**, 339–351, <https://doi.org/10.1175/JAMC-D-14-0204.1>.
- Mayson, R., 2019: *Port and the Douro*. 4th ed. Infinite Ideas Ltd., 416 pp.
- McCaffrey, K., and Coauthors, 2019: Identification and characterization of persistent cold pool events from temperature and wind profilers in the Columbia River basin. *J. Appl. Meteor. Climatol.*, **58**, 2533–2551, <https://doi.org/10.1175/JAMC-D-19-0046.1>.
- McKee, T. B., and R. D. O'Neal, 1989: The role of valley geometry and energy budget in the formation of nocturnal valley winds. *J. Appl. Meteor. Climatol.*, **28**, 445–456, [https://doi.org/10.1175/1520-0450\(1989\)028<0445:TROVGA>2.0.CO;2](https://doi.org/10.1175/1520-0450(1989)028<0445:TROVGA>2.0.CO;2).
- Miró, J. M., M. Pagès, and M. Kloßmann, 2010: Cold-air pool detection tools in the Pyrenees valleys. *14th Conf. on Mountain Meteorology*, Squaw Creek, CA, Amer. Meteor. Soc., 11.5, <https://ams.confex.com/ams/pdfpapers/173620.pdf>.
- , J. C. Peña, N. Pepin, A. Sairouni, and M. Aran, 2018: Key features of cold-air pool episodes in the northeast of the Iberian Peninsula (Cerdanya, eastern Pyrenees). *Int. J. Climatol.*, **38**, 1105–1115, <https://doi.org/10.1002/joc.5236>.
- Pagès, M., N. Pepin, and J. R. Miró, 2017: Measurement and modelling of temperature cold pools in the Cerdanya valley (Pyrenees), Spain. *Meteor. Appl.*, **24**, 290–302, <https://doi.org/10.1002/met.1630>.
- Pepin, N. C., M. K. Schaefer, and L. D. Riddy, 2009: Quantification of the cold-air pool in Kevo valley, Finnish Lapland. *Weather*, **64** (3), 60–67, <https://doi.org/10.1002/wea.260>.
- Pogue, K. R., and G. M. Dering, 2008: Temperature variations in the Walla Walla valley American viticultural area. *Proc. Seventh Int. Terroir Congress*, Agroscope Changins-Wädenswil, Nyon, Switzerland, IVES, 648–653, <https://people.whitman.edu/~pogue/geneva.pdf>.
- Reuter, H. I., A. Nelson, and A. Jarvis, 2007: An evaluation of void filling interpolation methods for SRTM data. *Int. J. Geogr. Inf. Sci.*, **21**, 983–1008, <https://doi.org/10.1080/13658810601169899>.
- Rupp, D. E., S. L. Shafer, C. Daly, J. A. Jones, and S. J. K. Frey, 2020: Temperature gradients and inversions in a forested Cascade Range basin: Synoptic-to local-scale controls. *J. Geophys. Res. Atmos.*, **125**, e2020JD032686, <https://doi.org/10.1029/2020JD032686>.
- Sluys, S. L., 2006: Climatic influences on the grapevine: A study of viticulture in the Waipara Basin. M.S. thesis, Dept. of Geography, University of Canterbury, 112 pp., <https://core.ac.uk/download/pdf/35458882.pdf>.
- Smart, W. M., 1990: *Textbook on Spherical Astronomy*. 6th ed. Cambridge University Press, 446 pp.
- Tarboton, D. G., 1997: A new method for the determination of flow directions and upslope areas in grid digital elevation models. *Water Resour. Res.*, **33**, 309–319, <https://doi.org/10.1029/96WR03137>.
- Ueckermann, M. P., R. D. Chambers, C. A. Brooks, W. E. Audette III, and J. Bieszczad, 2015: pyDEM: Global digital elevation model analysis. *Scipy 2015: 14th Python in Science Conf.*, Austin, TX, Enthought, Inc., 113–120, https://conference.scipy.org/proceedings/scipy2015/mattheus_ueckermann.html.
- Whiteman, C. D., 1990: Observations of thermally developed wind systems in mountainous terrain. *Atmospheric Processes over Complex Terrain*, *Meteor. Monogr.*, No. 45, Amer. Meteor. Soc., 5–42.
- , S. Zhong, W. J. Shaw, J. M. Hubbe, X. Bian, and J. Mittelstadt, 2001: Cold pools in the Columbia Basin. *Wea. Forecasting*, **16**, 432–447, [https://doi.org/10.1175/1520-0434\(2001\)016<0432:CPITCB>2.0.CO;2](https://doi.org/10.1175/1520-0434(2001)016<0432:CPITCB>2.0.CO;2).
- Zhong, S., X. Bian, and C. D. Whiteman, 2003: Time scale for cold-air pool breakup by turbulent erosion. *Meteor. Z.*, **12**, 229–233, <https://doi.org/10.1127/0941-2948/2003/0012-0231>.